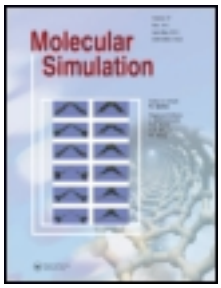

Molecular Simulation
Publication details, including instructions for authors and subscription information:
http://www.tandfonline.com/loi/gmos20

Wetting characterisation of silicon (1,0,0) surface

Murat Barisik [a] & Ali Beskok [a]
[a] Institute of Micro and Nanotechnology, Mechanical & Aerospace Engineering Department, Old Dominion University, Norfolk, VA, 23529-0247, USA
Version of record first published: 11 Feb 2013.

To cite this article: Murat Barisik & Ali Beskok (2013): Wetting characterisation of silicon (1,0,0) surface, Molecular Simulation, DOI:10.1080/08927022.2012.758854

To link to this article: http://dx.doi.org/10.1080/08927022.2012.758854

Molecular Simulation, 2013
http://dx.doi.org/10.1080/08927022.2012.758854

Taylor & Francis
Taylor & Francis Group

Wetting characterisation of silicon (1,0,0) surface

Murat Barisik and Ali Beskok*

Old Dominion University, Institute of Micro and Nanotechnology, Mechanical & Aerospace Engineering Department, Norfolk, VA 23529-0247, USA

(*Received 12 November 2012; final version received 7 December 2012*)

Water droplets on bare silicon surfaces are studied to examine the wetting behaviour as a function of the surface energy and to parameterise water–silicon interactions in order to recover the hydrophobic behaviour measured by experiments. Two different wetting regimes characterised by a critical interaction strength value are observed. At a threshold value of the water–silicon interaction parameter, water molecules start penetrating into the first layer of silicon surface under thermally vibrating walls, resulting in two distinct wetting behaviours. Fixed (cold) silicon walls do not exhibit the two different wetting characteristics. Size effects are studied for nano-scale droplets, and line tension influence is observed depending on the surface wettability. Decrease in the droplet size increases the contact angle values for the low wetting cases, while contact angles decrease for smaller droplets on the high wetting surfaces. Considering the line tension effects and droplet size, ε_{Si-O} for water–silicon interactions to recover the hydrophobic behaviour of silicon surfaces is estimated to be 12.5% of the value predicted using the Lorentz–Berthelot mixing rule.

Keywords: silicon–water interface; water nanodroplet; hydrophobic; hydrophilic; line tension

1. Introduction

Silicon and silicon-based materials as semi-conductors have been widely used in integrated circuits. Parallel to the technological developments, the transistor density on a single circuit has been increasing exponentially each year according to the prediction of Moore's Law [1]. The main driving mechanism, enabling current developments, is the micro- and nano-fabrication technologies providing higher packing densities. It was also Richard Feynman's vision 50 years ago, when he pointed out the necessity to understand the unique physics governing the matter in small scale [2]. Since then, micro- and nano-scale physics of silicon-based materials attracted greatest attention of scientists and engineers.

Molecular dynamics (MD) has been a strong tool providing an insight to the micro- and nano-scale world. A number of force fields have been proposed, which have been shown to provide accurate predictions for many molecular systems. However, the parameter values of the underlying force fields are still under investigation. There are numerous MD studies conducted on silicon (Si)-based materials [3,4]. Frequently, Si–Si interactions are modelled by many-body potentials enforcing the tetrahedral structure, while the van der Walls interactions of Si with other molecules are modelled using the two-body Lennard-Jones (LJ) potential. The potential parameters between pairs of identical molecules are obtained by *ab initio* methods. On the other hand, the interaction parameters of non-identical molecules are frequently calculated from the parameters of the pair of identical molecules by using the Lorentz–Berthelot mixing rule that utilises arithmetic mean for molecular diameter and geometric mean for the potential strength. For most systems, the interaction parameters between identical molecules are optimised for a bulk material system, which may need to be re-parameterised for the interaction of non-identical pairs instead of using the simple Lorentz–Berthelot mixing rule. Many authors indicate their concerns about the Lorentz–Berthelot mixing rule, and proposed ways to calculate the interaction parameters of non-identical molecules accurately [5,6]. One methodology is the measurement of water contact angle to define the interactions of water with carbon [7] and silica [8] surfaces for rigid solid surfaces.

The angle at which a liquid–vapour interface meets the solid surface is known as the contact angle. Even though the hydrophobic or hydrophilic nature of a surface should be defined by also considering other additional surface properties [9,10], contact angle can be utilised as a measure of the wetting phenomena, qualitatively. When a drop of liquid is on a solid surface, it may remain as a spherical drop or spread to cover the solid surface. Specifically, wetting occurs when the contact angle is less than 90°, while the liquid does not wet the surface for contact angle values greater than 90°. The wetting characteristic of silicon has been of great interest for a vast number of applications. From the earliest experimental studies, it was reported that the measured contact angle value is strongly dependent on the surface conditions of silicon. A thin layer (less than a 1 nm) of silicon dioxide

*Corresponding author. Email: abeskok@odu.edu

forms naturally on the surface when silicon is exposed to the ambient air. Hermansson et al. measured contact angles between 35° and 96° by varying the surface treatment that removed the native oxide layers on the surface at different amounts [11]. Silicon and thermally grown silicon dioxide are studied by Martinez by removing the native oxide formed on silicon with etching [12]. Water contact angle on silicon and silicon dioxide are reported to be 89° and 48°, respectively. Similarly, Arkles reported the contact angle between water and etched silicon between 86° and 88° [13]. In a recent study, Kim et al. measured the water contact angle as 70.1° on a bare silicon surface [14]. Through personal communications with the authors, they pointed out the difficulties of obtaining and maintaining a silicon surface without any chemical termination. The amount and the time scale of oxide layer growth were mentioned in [15], where freshly etched silicon exposed to air at room temperature is rapidly covered by a thin oxide layer of thickness 0.5 nm in a minute, followed with a logarithmic growth rate. Hence, the measured contact angle values in the literature differ with the thickness of the SiO_2 layer and experimental conditions. Bare silicon surface without any chemical termination is hydrophobic, while the oxidised layer adds hydrophilicity, based on the oxide layer's thickness. In this study, we use a contact angle value of 88° to compare with the MD calculated water contact angles on pure silicon surface.

Investigating the wetting behaviour of silicon surfaces was attempted by Yen to study the effect of different surface morphologies using MD [16]. Employing the parameters given in [17] and using fixed surfaces, the wetting properties of various surface conditions created by microstructures of various heights and spacing are examined, and also the contact angle on microstructured surface at a small range of silicon/water interaction strengths is studied [16]. This important study did not consider the effects of surface thermal vibrations and line tension, which are crucial to understand the correct wetting behaviour.

Our objective is to understand the wetting behaviour of thermally vibrating silicon (1,0,0) surface as a function of silicon–oxygen interaction strength. Starting with the classical mixing rules estimations, we varied the interaction parameters between silicon and water in order to match the microscopic contact angle calculated by MD with the experimentally measured macroscopic contact angle of 88°.

This paper is organised as follows. In Section 2, we explain the water model used in detail. Results of water in a periodic box are shown to recover experimental measurements of the radial distribution functions. In Section 3, we describe MD simulation details of silicon–water system and the interaction parameters used. After explaining the contact angle measurement methodology, we present the contact angle results for different interaction strength values. Detailed comparisons are made on density profiles near the surface in order to characterise the wetting behaviour of water on silicon. The same procedure is also performed for the droplet on a fixed (cold) wall, and effects of surface molecular vibrations are revealed in terms of the resulting contact angles and density profiles. Size dependency of calculated contact angle values is analysed to predict the corresponding macroscopic value for high and low surface energies by considering the influence of line tension. In the conclusions section, we present the proper Lennard-Jones (L-J) parameters to be used for recovering the macroscopic wetting behaviour of water on silicon.

2. Water model

Many different models for liquid water have been developed by fitting some physical properties of water; as a result, different models show agreement with the different properties of water. A model requiring more fitting parameters gives better results, but becomes computationally inefficient due to its complexity. On the other hand, many studies showed that the thermodynamic properties of water models were most sensitive to the van der Waals repulsive, short-range Coulomb and the polarisation components of the potential [18]. Thus, the model explaining the van der Waals and Coulombic interactions with a proper polarisation of water structure provide a fair understanding of complex water behaviour.

Water models can be classified by the number of points used to define the model, and whether the structure is treated as rigid or flexible. In our study, for the purpose of simplicity and computational efficiency, we chose extended simple point charge (SPC/E) model which can be described as effective rigid pair potentials composed of Lennard-Jones and Coulombic terms [19]. This water model has three interaction sites, corresponding to the three atoms of the water molecules. Each atom gets assigned a point charge to model the long-range Coulombic interactions, and the oxygen atom also exhibits L-J potential to model van der Waals forces. The truncated (6–12) L-J potential is given as

$$\Phi_{\text{truncated}}(r_{ij}) = 4\varepsilon\left(\left(\left(\frac{\sigma}{r_{ij}}\right)^{12} - \left(\frac{\sigma}{r_{ij}}\right)^{6}\right) - \left(\left(\frac{\sigma}{r_c}\right)^{12} - \left(\frac{\sigma}{r_c}\right)^{6}\right)\right), \quad (1)$$

where r_{ij} is the intermolecular distance, ε is the depth of the potential well, σ is the molecular diameter and r_c is the cut-off radius [20].

Table 1. Molecular interaction parameters utilised.

Molecule pair	σ (Å)	E (eV)	q (e)
O–O	3.166	0.006739	−0.8476
H–H	0	0	+0.4238
Si–Si	2.095	2.168201	0

SPC/E is a tetrahedral model with an OH bond length of 0.1 nm and H–O–H angle of 109.47°. SHAKE algorithm [21] is used to constrain the bond lengths and angle, thus making the model rigid. A short-range L-J term with a cut-off distance of 1 nm acts on the oxygen, while a charge q (0.4238e) is on each hydrogen, compensated by a charge $-2q$ (-0.8476e) on the oxygen. The long-range Coulombic part has been treated with a particle–particle particle-mesh (PPPM) solver which can handle long-range interactions for periodic systems with slab geometry more efficiently than the Ewald sum algorithm [22]. PPPM invokes a PPPM solver, which maps atom charge to a three-dimensional (3D) mesh, uses 3D fast Fourier transforms to solve Poisson's equation on the mesh, then interpolates electric fields on the mesh points back to the atoms. Water molecular parameters are given in Table 1. Newton's equations of motion were integrated using the Verlet algorithm with a time step of 0.001 ps. We use Large-Scale Atomic/Molecular Massively Parallel Simulator [23] as our MD solver.

2.1 Water in a periodic box

We simulated water with 792 H_2O molecules in a box of $2.2 \times 4.5 \times 2.4$ nm dimensions ($x \times y \times z$ directions) corresponding to a density of 0.9972 g/cm^3. The periodicity boundary condition was applied in all directions. Simulation was started from the Maxwell–Boltzmann velocity distribution for all molecules at 300K. NVT (constant number of the molecules, constant volume and constant temperature) ensemble was used initially with the Nose–Hoover thermostat maintaining the system temperature at 300 K, and ran the simulation for 2 ns. Then, we assigned NVE (constant number of the molecules, constant volume and constant energy) system and checked temperature and energy changes to ensure that the system has reached equilibrium for another 1 ns. After which, time averaging of desired properties was performed for 4 ns. Longer time averaging was also performed to confirm the convergence of density and temperature profiles to steady state.

The radial distribution function describes how the atomic density varies as a function of the distance from one particular atom. The radial distribution functions, g_{OO}, g_{OH} and g_{HH}, are commonly used when the structure of the liquid water is studied. These intermolecular partial pair correlation functions for liquid water at 25°C were determined from neutron diffraction data by Soper and Phillips [24]. The radial distribution functions computed from our simulations for SPC/E water model is compared with the experimental results as shown in Figure 1. Calculated radial distribution functions are in good agreement with the experimental results, validating the SPC/E model.

3. Water droplet on silicon surface

Simulation domain is formed by two silicon slabs and a nano-scale water droplet, as illustrated in Figure 2(a). The bottom silicon slab consisting of 74,303 silicon molecules with dimensions of $27.15 \times 27.15 \times 1.3$ nm in $x \times y \times z$ directions is designed to study the wetting behaviour. Silicon surface is modelled as diamond cubic structure with (0,0,1) crystal plane facing the fluid. Top silicon slab is $27.15 \times 27.15 \times 0.27$ nm in $x \times y \times z$ directions and located 20 nm away from the bottom surface parallel to the xy-plane. Periodicity boundary conditions were applied in the vertical (x) and lateral (y) directions. Atoms in the top and in the outermost two layers of the bottom silicon surface were fixed to their original locations to maintain a fixed volume system, while the remaining atoms throughout the domain were free to move. Si–Si interactions were calculated by Stillinger–Weber potential which considers two-body interactions with an additional many-body dependence [25]. The water droplet was formed using 2744 water molecules in initially rectangular shape, and was centred on top of the main silicon surface 0.4 nm away between the two slabs. We ensured that the simulation domain size was large enough to prevent any effects on the droplet. SPC/E water molecules interact with silicon surface only by van der Waals interactions of silicon and oxygen using a cut-off distance of 1 nm. The L-J parameters for silicon–oxygen interactions can be calculated by L–B mixing rule given as

$$\sigma_{Si-O} = \frac{\sigma_{Si-Si} + \sigma_{O-O}}{2}, \varepsilon_{Si-O} = \sqrt{\varepsilon_{Si-Si} \times \varepsilon_{O-O}}. \quad (2)$$

Using the corresponding parameters given in Table 1, L–B mixing rule predicts the interaction parameters $\overset{*}{\sigma}_{Si-O} = 2.6305$ Å and $\overset{*}{\varepsilon}_{Si-O} = 0.12088$ eV. As discussed earlier, we utilised different ε_{Si-O} values to understand the wetting characteristic of silicon and to match the microscopic contact angle with the experimental macroscopic wetting angle after proper modelling of the droplet size effects. Thus, we utilised ε_{Si-O} values of $0.05\times$, $0.1\times$, $0.125\times$, $0.15\times$, $0.2\times$, $0.4\times$, $0.7\times$ and $1\times \overset{*}{\varepsilon}_{Si-O}$.

Equilibrium between the water droplet and its surroundings forms according to the surface tension and internal pressure of droplet at the specified temperature. Occasionally, spontaneous evaporation from the droplet

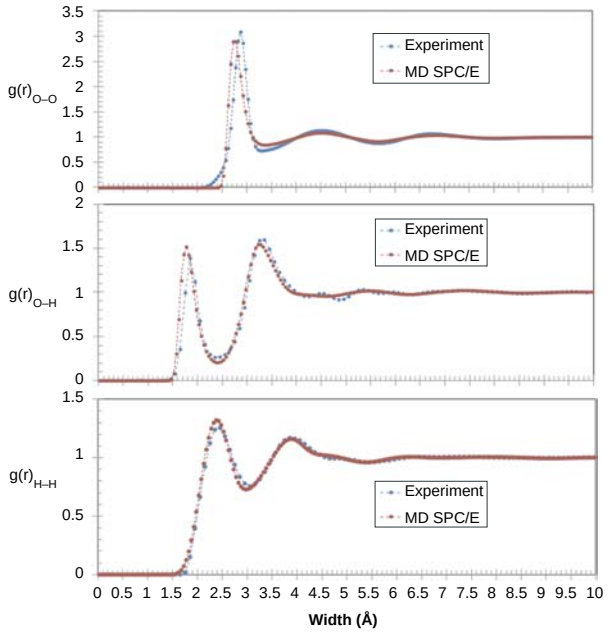

Figure 1. (Colour online) Comparison of the MD calculated water radial distributions for O–O, O–H and H–H at 300 K with experimental measurements of Soper et al. [21].

into the vacuum may take place. In such cases, very few water molecules escape from the droplet, have free flight or multiple collisions with the silicon surfaces and meet with the main body of the droplet again. During this behaviour, the number of escaped molecules remains constant through the simulation time period, and the volume of the cluster remains effectively constant.

Simulations were started from the Maxwell–Boltzmann velocity distribution for all molecules at 300 K. NVT ensemble was applied with Nosé–Hoover thermostat keeping the system at 300 K. Initial particle distribution was evolved 10^6 time steps (1 ns) to reach an isothermal steady state using 1 fs time steps. After which, time averaging of the desired properties was performed for 5×10^5 additional time steps (0.5 ns). Longer time averaging has also been performed to confirm the convergence of results to steady state. The computational domain is divided into rectangular bin structures with the size of $0.2 \times 0.2 \times 0.1$ nm in $x \times y \times z$ directions. Data were sampled every 5 ps during the 500 ps time averaging period. Centre of the droplet at each snapshot (result of 5 ps sampling) in 3D space was identified. All samples are averaged after matching their centre locations to compensate for droplet motion on the surface due to diffusion.

3.1 Contact angle

The 3D structure of the water droplet was found to be spherical except in the near wall region. Density values were calculated in 2D x–z and y–z planes passing through the droplet centre, normal to the surface. Similar density profiles were found confirming the symmetric spherical shape of the droplet. Figure 2(a) shows the computation of the contact angle, while the density contours in xz-plane is shown in Figure 2(b). Oxygen, hydrogen and the silicon molecules are illustrated as red, white and yellow spheres, respectively. First, the droplet boundary was determined as the points at which the density is half of bulk water (0.5 g/cm^3). Second, we fit a circle passing through the points 8 Å above the surface. Near wall density points closer to surface than 8 Å were omitted to avoid the influence from density fluctuations at the liquid–solid interface. Finally, we extrapolated the circular fit to the silicon surface where the contact angle (θ) is computed. Using the calculated droplet properties, θ can be defined as

$$\begin{aligned} \theta &= \pi + \arccos\left(\tfrac{r_B}{r}\right), \quad \text{if } H > 0, \\ \theta &= \pi - \arccos\left(\tfrac{r_B}{r}\right), \quad \text{if } H < 0 \end{aligned} \tag{3}$$

where r is the droplet radius, r_B is the base radius of droplet on silicon surface and H is the distance between the droplet

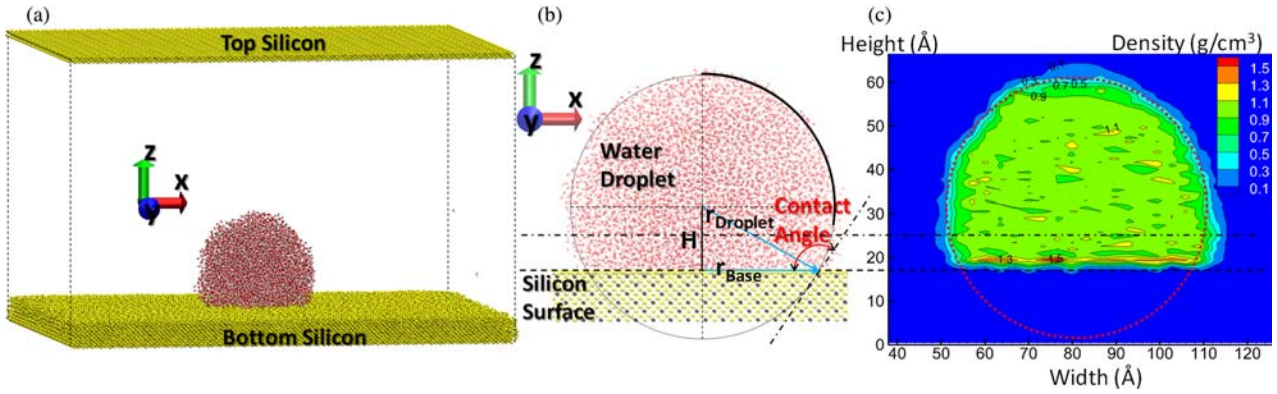

Figure 2. (Colour online) (a) The snapshot of simulation domain consisting of two silicon slabs and water nano-droplet. (b) Schematic for the computation of contact angle with the snapshot of $0.1 \times \varepsilon^*_{Si-O}$ case at the background. Oxygen, hydrogen and silicon molecules are illustrated as red, white and yellow spheres, respectively. (c) Density contours in the x–z plane of the same case.

centre and the silicon surface, as illustrated in Figure 2(a). H can be positive or negative depending on the droplet centre being over or under the silicon surface.

3.2 Wetting behaviour of the silicon (1,0,0) surface

The next step was to characterise the wetting behaviour of silicon. Water droplets were formed on the thermally vibrating silicon surface at different ε_{Si-O} values which are on the order of the value calculated by L–B ($\varepsilon^{*}_{Si-O} = 0.12088\,eV$) as 1, 0.7, 0.4, 0.2, 0.15, 0.125, 0.1 and $0.05 \times \varepsilon^{*}_{Si-O}$. Figure 3(a)–(h) shows the snapshot of these eight cases with illustrations of the contact angle measurements. Using the L–B mixing rule ($\varepsilon_{Si-O}/\varepsilon^{*}_{Si-O} = 1$) resulted in 25.6° wetting angle of water with thermally active silicon walls, which is a high wetting behaviour. The contact angle increases with decreased interaction strength from the L–B prediction; as a result, the wettability changes from high to low. With decreased wettability, height of the water droplet increases leading to a higher contact angle with lower droplet and contact radius. Calculated contact angle values as a function of the Si–O interaction strength are presented in Table 2.

The contact angle variation as a function of $\varepsilon_{Si-O}/\varepsilon^{*}_{Si-O}$ is plotted in Figure 4. Similar to earlier MD studies [7,16,26], the contact angle decreases linearly with increased interaction strength. However, we observed two different wetting regimes characterised by a critical value of Si–O interaction strength ($\varepsilon_{Si-O\,critical}$), as illustrated in Figure 4. For $\varepsilon_{Si-O} < \varepsilon_{Si-O\,critical}$, linear change in contact angle is steeper than the cases with $\varepsilon_{Si-O} > \varepsilon_{Si-O\,critical}$, where $\varepsilon_{Si-O\,critical}$ is calculated to be $0.18 \times \varepsilon^{*}_{Si-O}$.

In order to understand these two different wetting regimes better, we investigated the variation of water density for each case. Density values measured along the centre line of each droplet normal to the surface are plotted in Figure 5(a). Density layering with two distinct peak points was observed on the surface [27], although it becomes more profound with increased ε_{Si-O}. The density values converge to the constant water density of $1\,g/cm^3$ after 8 Å distance away from the surface. Height of the droplets can be defined as the point where the density goes to zero with a rapid decrease away from the surface. Increase in ε_{Si-O} increases wetting, and hence, height of the droplets on the silicon surface decreases. Interestingly, we observed diffusion of the water particles into the silicon surface for high ε_{Si-O} values. Figure 5(b) gives a closer view of the density profiles in the 13–26 Å range. For $\varepsilon_{Si-O} \geq 0.2 \times \varepsilon^{*}_{Si-O}$, water penetrates into the gap between the first and second silicon layers, and the water density in this region increases with increased ε_{Si-O}. This is the main reason of two distinct wetting regimes that water diffuses into the silicon for $\varepsilon_{Si-O} > \varepsilon_{Si-O\,critical}$, while this diffusion is negligible for the lower values. Figure 5(c),(d) shows zoomed view of the near wall region for

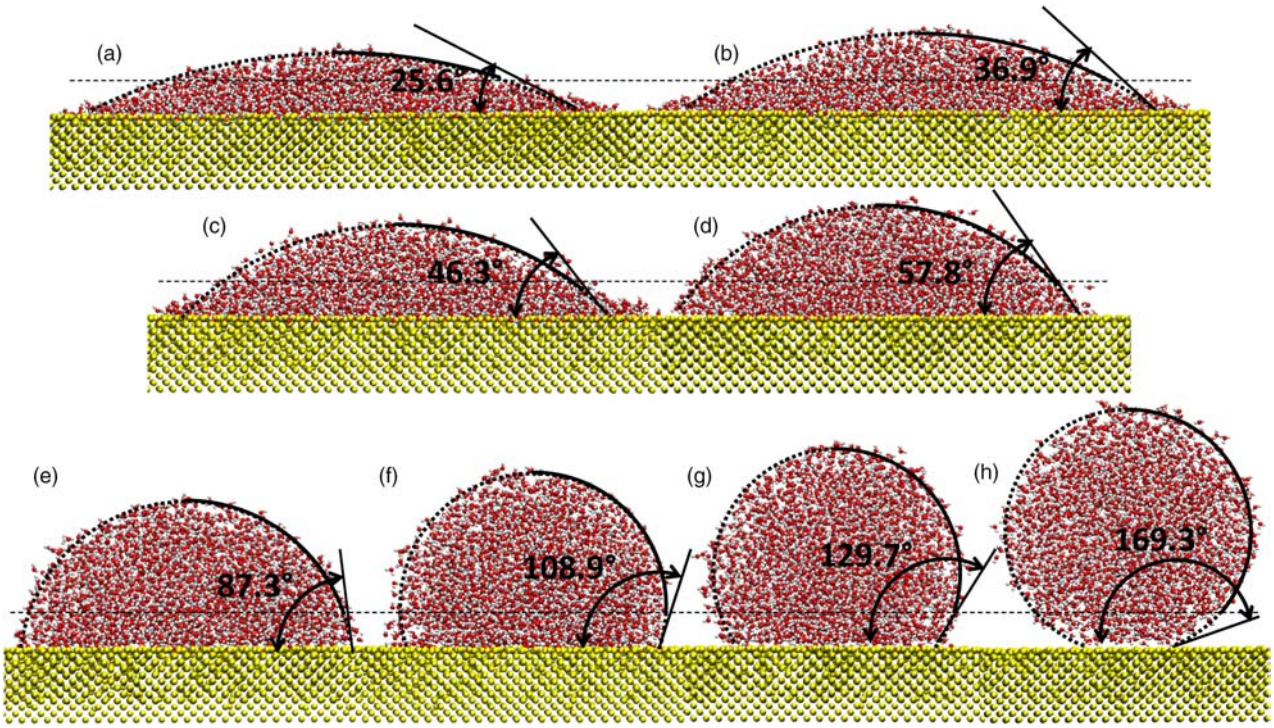

Figure 3. (Colour online) Snapshots of water droplets on thermally vibrating silicon surface with the interaction strength values of 1, 0.7, 0.4, 0.2, 0.15, 0.125, 0.1 and $0.05 \times \varepsilon^{*}_{Si-O}$, respectively. Lorentz–Berthelot mixing rule gives $\varepsilon^{*}_{Si-O} = 0.12088\,eV$.

Table 2. Calculated contact angle values as a function of the Si–O interaction strength.

Case	ε_{Si-O} (eV)	$\varepsilon_{Si-O}/\varepsilon^{*}_{Si-O}$	Contact angle (°)
1	0.12088	1	25.6
2	0.084616	0.7	36.9
3	0.048352	0.4	46.3
4	0.024176	0.2	57.8
5	0.018132	0.15	87.3
6	0.01511	0.125	108.9
7	0.012088	0.1	129.7
8	0.006044	0.05	169.3

$\varepsilon_{Si-O} = 0.1 \times \varepsilon^{*}_{Si-O}$ and $\varepsilon_{Si-O} = 0.2 \times \varepsilon^{*}_{Si-O}$ interfaces. Silicon molecules were reduced in size to observe the diffused water molecules better. Only hydrogen molecules (white spheres) can penetrate at $\varepsilon_{Si-O} = 0.1 \times \varepsilon^{*}_{Si-O}$, which explains negligible water density (different than zero) measured inside the surface. However, both oxygen (red spheres) and hydrogen (white) molecules can slip into the gap for the $\varepsilon_{Si-O} = 0.2 \times \varepsilon^{*}_{Si-O}$ case. Penetration of oxygen, which has 16 times larger atomic weight than hydrogen, creates a different wetting behaviour.

3.3 *Effect of wall vibrations*

In this study, silicon molecules inside the region 1.1 nm away from the interface are free to move while they interact with Stillinger–Weber potential. On the other hand, the silicon surface may be treated as a frozen solid structure where all solid molecules are fixed to their original positions. By this way, Si–Si interactions are discarded; and hence, the computational burden is reduced significantly. Many MD contact angle studies used the frozen wall technique and reported negligible effects on the resulting droplet shape [7,28]. In order to clarify the wall vibration effects, we compare the droplets formed on a frozen and on a thermally vibrating silicon surface, as shown in Figure 6. On the left sides of Figure 6(a)–(c), we present droplets formed on a thermally vibrating silicon surface, where only the two outermost layers are fixed and the remaining silicon molecules vibrate at 300 K. Except the very first layer facing the droplet, silicon molecules retained their native diamond cubic structure. The droplets on the fixed surfaces are given on the right sides of Figure 6(a)–(c). Comparisons between the thermally vibrating and fixed surfaces clearly indicate substantial change in the wetting behaviour.

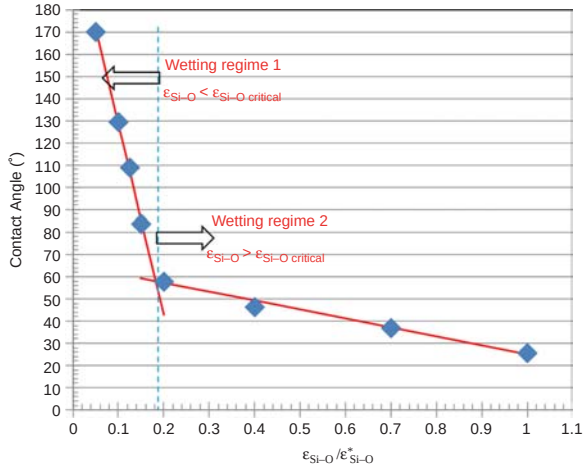

Figure 4. (Colour online) Contact angle variation as a function of $\varepsilon_{Si-O}/\varepsilon^{*}_{Si-O}$. Two different linear fits are applied on the wetting regimes 1 and 2.

Contrary to the thermally vibrating wall cases, we observed a different wetting behaviour on fixed surfaces. Calculated contact angles on the fixed wall are plotted as a function of ε_{Si-O} in Figure 6(d) along with the data for the vibrating wall cases. For the $\varepsilon_{Si-O} < \varepsilon_{Si-O\,critical}$, contact angles of the fixed surface are found to be higher than the results of the thermally vibrating case (Figure 6(a)) while the change in the contact angle with ε_{Si-O} shows a linear variation similar to the wetting regime 1. However, when the ε_{Si-O} exceeds the $\varepsilon_{Si-O\,critical}$, wetting behaviour diverges from the earlier results of the second regime. With increased ε_{Si-O}, contact angles decrease rapidly, similar to the behaviour in regime 1, resulting in complete wetting of the silicon surface for $\varepsilon_{Si-O} = 0.4 \times \varepsilon^{*}_{Si-O}$.

Density profiles along the centre line of droplets normal to the fixed surface are plotted in Figure 7 for different $\varepsilon_{Si-O}/\varepsilon^{*}_{Si-O}$. Droplets formed on the fixed surface have larger heights than those formed on the vibrating surface for 0.05, 0.1 and $0.15 \times \varepsilon^{*}_{Si-O}$. However, starting with $0.4 \times \varepsilon^{*}_{Si-O}$, droplet heights suddenly decrease indicating complete wetting of the surface. A closer view of the near wall region given in Figure 7(b) shows the formation of a third distinct density layer at close proximity to the fixed surface for $\varepsilon_{Si-O} > \varepsilon_{Si-O\,critical}$ cases. In addition, density peak values are higher than the corresponding vibrating wall cases. More interestingly, water molecules cannot penetrate under the first layer of the fixed surface. In the case of a vibrating wall, water can diffuse into the surface, which increases the droplet contact area and the interfacial energy, and hence, yields decreased wettability for $\varepsilon_{Si-O} > \varepsilon_{Si-O\,critical}$. However, using fixed surface expels such surface roughness produced by the corrugations of vibrating molecules and creates 'an atomistically flat surface' which is more hydrophilic than the vibrating wall case. Therefore, a fixed surface leads to a wrong physical behaviour in the silicon–water system. In modelling dynamic processes such as wetting, transfer of momentum between the solid and liquid is a critical factor, and accurate modelling is important to capture correct molecular mechanisms.

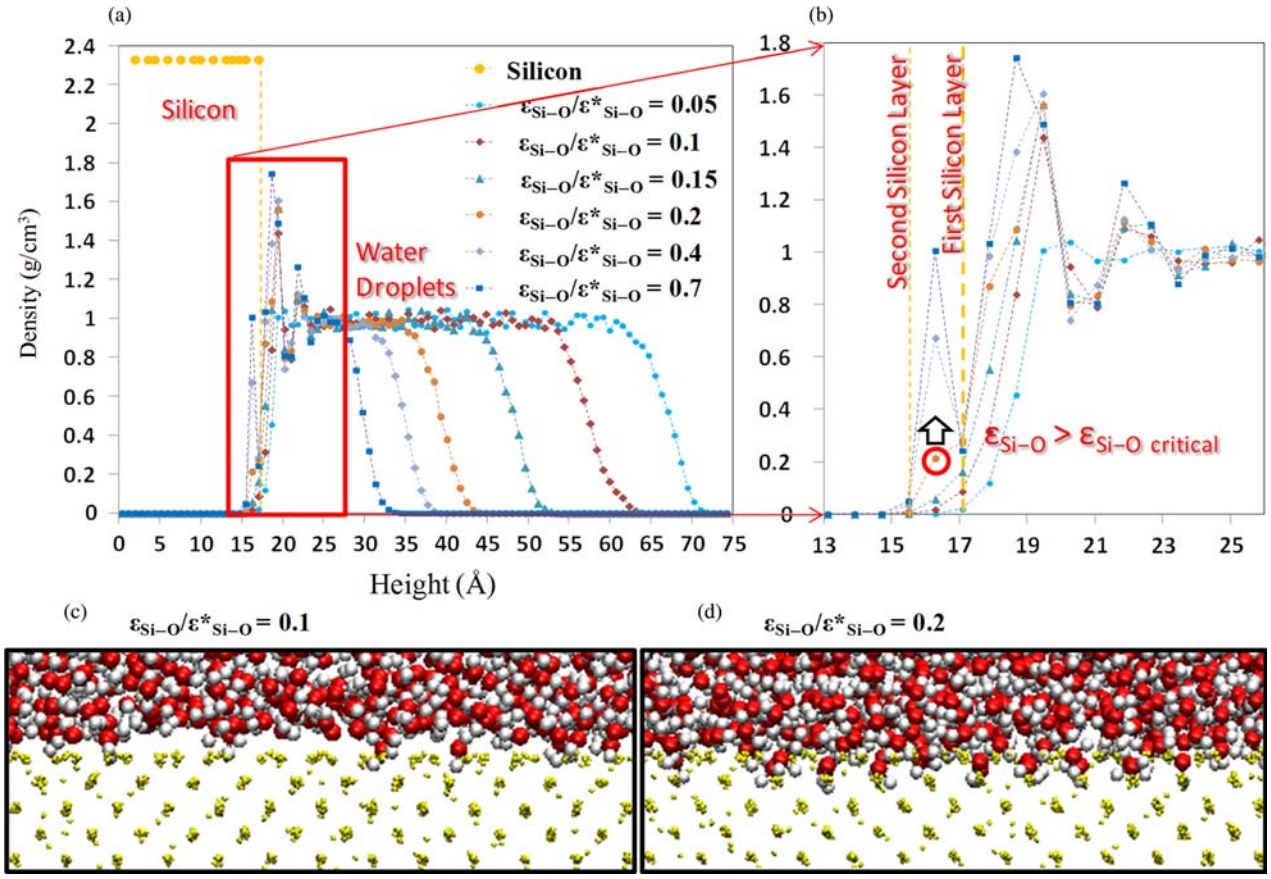

Figure 5. (Colour online) (a) Density profiles along the centre line of droplets normal to the surface for different $\varepsilon_{Si-O}/\varepsilon^*_{Si-O}$ cases. (b) Closer view of the density profiles in the 13–26 Å range. (c) and (d) Comparison of $\varepsilon_{Si-O} = 0.1 \times \varepsilon^*_{Si-O}$ and $0.2 \times \varepsilon_{Si-O}$ interfaces. Molecular size of silicon is reduced to show the diffusion of hydrogen (white) and oxygen (red) molecules on the silicon surface.

Macroscopic contact angle versus microscopic contact angle

The equilibrium at the solid–liquid–vapour interface is defined by Young's modulus equation as

$$\gamma_{SV} = \gamma_{SL} + \gamma_{LV} \cos\theta_\infty, \tag{4}$$

where γ_{SV}, γ_{SL} and γ_{LV} are the interfacial tensions at the boundaries between liquid (L), solid (S) and vapour (V), while θ_∞ is the contact angle for a macroscopic droplet. As the droplet size decreases, three-phase interactions at the contact line between liquid, solid and vapour cannot be simply explained by the interfacial tensions of each pair. In addition to the interfacial and surface tensions, line tension along which the three interfaces meet becomes increasingly important. An additional energy per unit length of the contact line at the foot of the droplet contributes to the free energy of the droplet and yields the modified Young's modulus equation [29].

$$\gamma_{SV} = \gamma_{SL} + \gamma_{LV} \cos\theta + \frac{\tau}{r_B}, \tag{5}$$

where τ is the line tension between the droplet and surface and r_B is the droplet base radius. For $r_B \to \infty$, microscopic contact angle, θ, can be defined in terms of the macroscopic contact angle as

$$\cos\theta = \cos\theta_\infty - \frac{\tau}{\gamma_{LV}} \frac{1}{r_B}, \tag{6}$$

where $\cos\theta$ term is linearly related to the droplet base curvature $1/r_B$. For droplets smaller than 100 nm, line tension effects cannot be neglected [30]. Experimental studies reported the line tension effects for nanometer to micrometer size droplets [31]. According to Equation (6), the microscopic contact angle deviates from the macroscopic angle due to the line tension. With a decrease in the droplet size, positive line tension contracts the droplet and increases the contact angle, whereas a negative line tension enhances wetting.

In order to examine the size dependence of the calculated microscopic contact angle values, simulations were performed with droplets consisting of 9261, 5832, 2744 and 1331 water molecules at different interaction

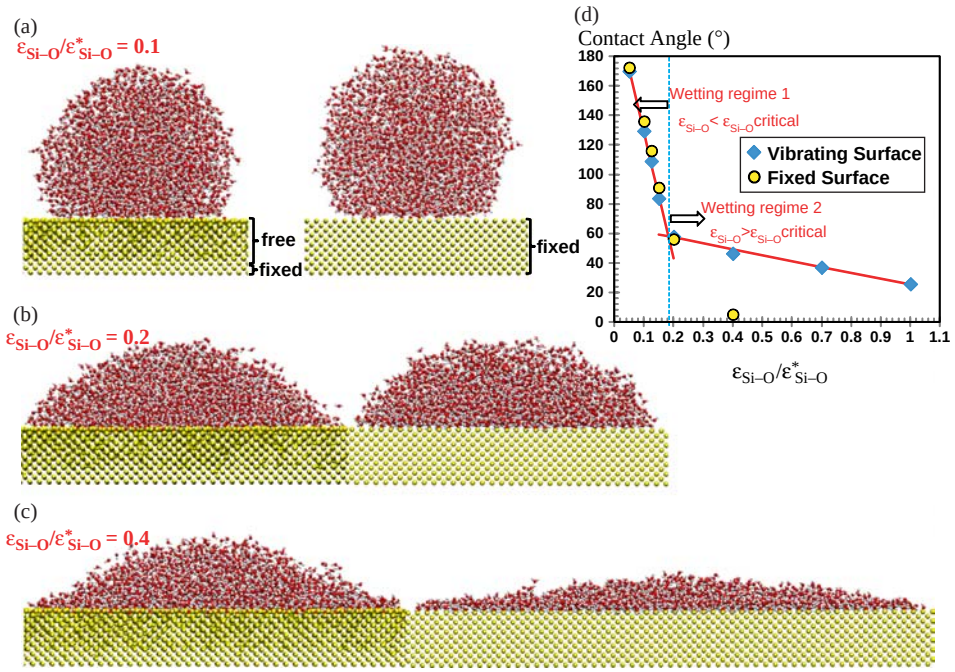

Figure 6. (Colour online) (a)–(c) Comparison of the water droplet snapshots on the thermally vibrating (left) and on the fixed silicon surfaces (right) with the interaction strength values of 0.1, 0.2 and $0.4 \times \varepsilon^*_{Si-O}$. (d) Variations of contact angles on the fixed and vibrating walls as a function of ε_{Si-O}.

values of 0.1, 0.125 and $0.4 \times \varepsilon^*_{Si-O}$. The 0.1 and $0.125 \times \varepsilon^*_{Si-O}$ cases have low surface energy and exhibits hydrophobic behaviour, while the $0.4 \times \varepsilon^*_{Si-O}$ case has high energy surface which behaves hydrophilically. The droplets with different sizes are illustrated in Figure 8, and the contact angle values are given in Table 3. An increase in the droplet size decreased the contact angle values for $\varepsilon_{Si-O} = 0.1$ and $0.125 \times \varepsilon^*_{Si-O}$ cases (Figure 8(a)). For a low wetting surface, smaller droplets with fewer molecules resulted in weaker molecular interactions with the surface through the contact line having a positive curvature (concave upward). Hence, cohesive forces originating from the water–water molecular interactions became dominant in small droplets and resulted in a contraction of

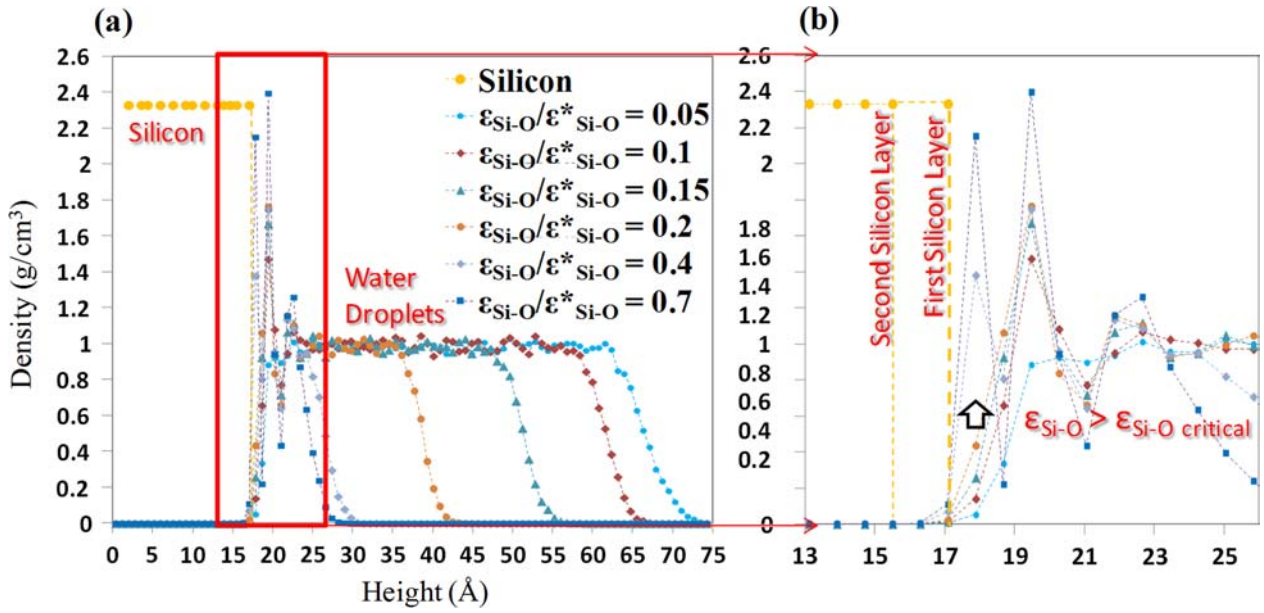

Figure 7. (Colour online) (a) Density profiles along the centre line of droplets normal to the fixed silicon surface for different $\varepsilon_{Si-O}/\varepsilon^*_{Si-O}$ values. (b) Zoomed view of the density profiles in 13–26 Å range.

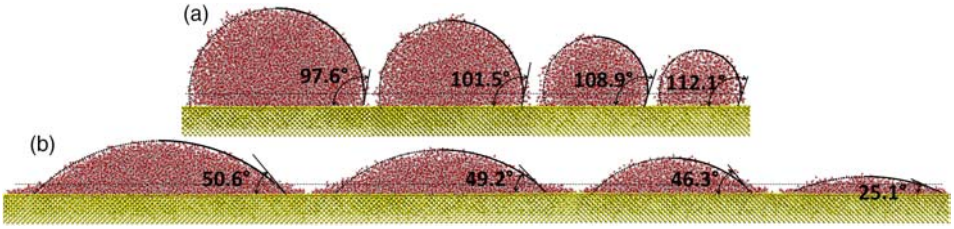

Figure 8. (Colour online) Droplets with 9261, 5832, 2744 and 1331 water molecules (from left to right) on (a) low ($\varepsilon_{Si-O} = 0.125 \times \varepsilon^{*}_{Si-O}$) and (b) high ($\varepsilon_{Si-O} = 0.4 \times \varepsilon^{*}_{Si-O}$) energy surfaces.

the droplet and a higher contact angle value. On the contrary, increasing the droplet size increased the contact angles for the $\varepsilon_{Si-O} = 0.4 \times \varepsilon^{*}_{Si-O}$ case (Figure 8(b)). In practice, a high energy surface (hydrophilic) spreads the droplet creating a longer contact line length with a negative curvature (convex upward). When the droplet size is reduced, cohesive forces are weakened due to the limited number of water molecules forming the dome of the droplet. Thus, the smaller droplet spreads further and creates a lower contact angle on the high wetting surface.

In Figure 9, cosine of the contact angle for different sized droplets is plotted as a function of the droplet base radius $1/r_B$ for 0.1, 0.125 and $0.4 \times \varepsilon^{*}_{Si-O}$ cases. Linear fits were applied on each group of droplets at the same ε_{Si-O}. Slope of each linear fit is proportional to τ according to Equation (6). Low wetting surface case had negative slope indicating a positive line tension, while high wetting surfaces created positive slopes with negative line tension. Using the corresponding slope values of each line, the line tensions were predicted as 0.35×10^{-10} N ($0.1 \times \varepsilon^{*}_{Si-O}$ case), 0.64×10^{-10} N ($0.125 \times \varepsilon^{*}_{Si-O}$ case) and -0.45×10^{-10} N ($0.4 \times \varepsilon^{*}_{Si-O}$ case) by assuming a constant water surface tension of 72 mN/m [7]. Calculated line tension values are in the range of experimental measurements [29,31].

By extending the linear fits to the limit of infinitely large droplets ($1/r_B = 0$), we predicted the macroscopic contact angle values as 112.7°, 87.9° and 56.4° for $\varepsilon_{Si-O} = 0.1$, 0.125 and $0.4 \times \varepsilon^{*}_{Si-O}$ cases, respectively. In order for water droplet to recover the macroscopic contact angle on the silicon surface, an appropriate estimate for the interaction strength value was found as $\varepsilon_{Si-O} = 0.125 \times \varepsilon^{*}_{Si-O}$ for the current simulation models of silicon (Stillinger–Weber) and water (SPC/E). This interaction strength value is used in further studies that involve Si–O pairs.

4. Conclusions

Our findings showed that the interaction parameters for silicon–water system should be properly tuned in order to recover the wetting behaviour measured by experiments. Using L–B mixing rule is not suitable to capture correct interface interactions in which the parameters predicted by L–B mixing rule created a high wetting surface opposite to the real hydrophobic nature of silicon.

We confirmed that the contact angle is exclusively related to the surface energy which is a function of the silicon–water interaction strength (ε_{Si-O}). With a systematic study of silicon surfaces at different ε_{Si-O}, two different wetting regimes were observed depending on a critical ε_{Si-O} value ($\varepsilon_{Si-O\,critical}$). Specifically, silicon was hydrophobic and contact angles showed a strong dependence on the surface energy for $\varepsilon_{Si-O} < \varepsilon_{Si-O\,critical}$. On the contrary, hydrophilic behaviour was observed for $\varepsilon_{Si-O} > \varepsilon_{Si-O\,critical}$, and dependence of contact angles on ε_{Si-O} was weaker. Diffusion of water molecules into silicon is the main reason for different wetting behaviours according to $\varepsilon_{Si-O\,critical}$. For $\varepsilon_{Si-O} > \varepsilon_{Si-O\,critical}$ cases, water penetrated under the first layer of silicon increasing the droplet contact area and the interfacial energy, resulting in increased hydrophobicity. However, such behaviour (diffusion of water) was not observed for the cases where fixed silicon surfaces having no thermal vibrations were employed. As a result, using vibrating wall model is crucial to estimate the wetting behaviour correctly.

Line tension influence was observed as a size effect for the studied nano-scale droplets. Low wetting surfaces

Table 3. Calculated contact angles of different sized droplets for $\varepsilon_{Si-O} = 0.1$, 0.125 and $0.4 \times \varepsilon^{*}_{Si-O}$.

	$\varepsilon_{Si-O} = 0.1 \times \varepsilon^{*}_{Si-O}$		$\varepsilon_{Si-O} = 0.125 \times \varepsilon^{*}_{Si-O}$		$\varepsilon_{Si-O} = 0.4 \times \varepsilon^{*}_{Si-O}$	
No. water molecules	r_B (Å)	θ (°)	r_B (Å)	θ (°)	r_B (Å)	θ (°)
1331	12.74	139.1	20.65	112.1	43.69	25.1
2744	20.21	129.6	27.19	108.9	44.98	46.3
5832	27.43	126.6	38.79	101.5	63.32	49.2
9261	36.18	119.1	47.77	97.6	74.26	50.6
∞	∞	112.7	∞	87.9	∞	56.4

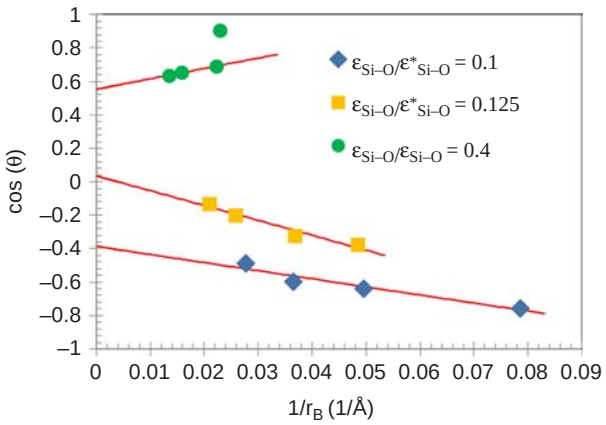

Figure 9. (Colour online) Cosine of the contact angle for different sized droplets as a function of the droplet base radius $1/r_B$ for the 0.1, 0.125 and $0.4 \times \varepsilon^*_{Si-O}$ cases.

developed positive line tension, which increased the contact angle with a decrease in the droplet size. Oppositely, negative line tension formed on the high wetting surface, which decreased the contact angle for smaller droplets. Using the modified Young's modulus equation, contact angles were predicted for the macroscopic limit. Silicon–water (Si–O) interaction strength was estimated as $\varepsilon_{Si-O} = 0.125 \times \varepsilon^*_{Si-O}$, which developed macroscopic contact angle of 87.9°, capturing the experimental wetting behaviour of pure silicon surface. The predicted value will be used for the investigation of thermal resistance on the silicon–water interface.

Acknowledgements

This work was supported by the National Science Foundation under Grant No: CBET 0931988. The authors would like to thank the Extreme Science and Engineering Discovery Environment (XSEDE) supported by the National Science Foundation grant number OCI 1053575 for computing resources.

References

[1] G.E. Moore, *Cramming more components onto integrated circuits*, Proc. IEEE 86 (1998), pp. 82–85.
[2] R.P. Feynman, *There's plenty of room at the bottom*, Eng. Sci. 23 (1960), pp. 22–36.
[3] Y. Qiu, Y. Chen, L. Liu, and G. Zhao, *Water and ion distributions in a silicon nanochannel a molecular dynamics study*, Proc. Inst. Mech. Eng. Part N: J. Nanoeng. Nanosyst. 226 (2012), pp. 31–34.
[4] J. Jingchun, S. Liu, and X. Yang, *Molecular dynamics simulation of wetting on modified amorphous silica surface*, Appl. Surf. Sci. 255 (2009), pp. 9078–9084.
[5] A.K. Al-Matar and D.A. Rockstraw, *A generating equation for mixing rules and two new mixing rules for interatomic potential energy parameters*, J. Comput. Chem. 15 (2004), pp. 660–668.
[6] M. Fyta and R.R. Netz, *Ionic force field optimization based on single-ion and ion-pair solvation properties: Going beyond standard mixing rules*, J. Chem. Phys. 136 (2012), p. 124103.
[7] T. Werder, J.H. Walther, R.L. Jaffe, T. Halicioglu, and P. Koumoutsakos, *On the water–carbon interaction for use in molecular dynamics simulations of graphite and carbon nanotubes*, J. Phys. Chem. B 107 (2003), pp. 1345–1352.
[8] E.R. Cruz-Chu, A. Aksimentiev, and K. Schulten, *Water–silica force field for simulating nanodevices*, J. Phys. Chem. B 110 (2006), pp. 21497–21508.
[9] L. Gao and T.J. McCarthy, *Teflon is hydrophilic. Comments on definitions of hydrophobic, shear versus tensile hydrophobicity, and wettability characterization*, Langmuir 24 (2008), pp. 9183–9188.
[10] T.A. Ho, D.V. Papavassiliou, L.L. Lee, and A. Striolo, *Liquid water can slip on a hydrophilic surface*, PNAS 108 (2011), pp. 16170–16175.
[11] K. Hermansson, U. Lindberg, B. Hok, and G. Palmskog, *Wetting properties of silicon surfaces*, Proceedings of the IEEE International Conference on Solid-State Sensors Actuators, IEEE, San Francisco, CA, 1991, pp. 193–196.
[12] N. Martinez, *Wettability of silicon, silicon dioxide, and organosilicate glass*, Master of Science thesis, University of North Texas, 2009.
[13] B. Arkles, *Hydrophobicity, hydrophilicity and silanes*, Paint Coatings Industry Magazine, October (2006).
[14] B.S. Kim, S. Shin, S.J. Shin, K.M. Kim, and H.H. Cho, *Micro-nano hybrid structures with manipulated wettability using a two-step silicon etching on a large area*, Nano. Res. Lett. 6 (2011), pp. 333–343.
[15] I.J. Haller, *Covalently attached organic monolayers on semiconductor surfaces*, Am. Chem. Soc. 100 (1978), pp. 8050–8055.
[16] T.H. Yen, *Wetting characteristics of nanoscale water droplet on silicon substrates with effects of surface morphology*, Mol. Simul. 37 (2011), pp. 766–778.
[17] R. Qiao and N.R. Aluru, *Ion concentrations and velocity profiles in nanochannel electroosmotic flows*, J. Chem. Phys. 118 (2003), pp. 4692–4702.
[18] T.D. Iordanov, G.K. Schenter, and B.C. Garrett, *Sensitivity analysis of thermodynamic properties of liquid water: A general approach to improve empirical potentials*, J. Phys. Chem. A 110 (2006), pp. 762–771.
[19] H.J.C. Berendsen, J.R. Grigera, and T.P.J. Straatsma, *The missing term in effective pair potentials*, Phys. Chem. 91 (1987), pp. 6269–6271.
[20] M.P. Allen and D.J. Tildesley, *Computer Simulation of Liquids*, Oxford Science Publications Oxford University Press, New York, 1989.
[21] S. Miyamoto and P.A. Kollman, *Settle: An analytical version of the shake and rattle algorithm for rigid water models*, J. Comput. Chem. 13 (1992), pp. 952–962.
[22] S.J. Plimpton, R. Pollock, and M. Stevens, *Particle-mesh Ewald and rRESPA for parallel molecular dynamics simulations*, Proceedings of the Eighth SIAM Conference on Parallel Processing for Scientific Computing, SIAM, Philadelphia, PA, 1997, pp. 8–21.
[23] S.J. Plimpton, *Fast parallel algorithms for short-range molecular dynamics*, J. Comput. Phys. 117 (1995), pp. 1–19, see http://lammps.sandia.gov for more information.
[24] A.K. Soper and M.G. Phillips, *A new determination of the structure of water at 25°*, Chem. Phys. 107 (1986), pp. 47–60.
[25] F.H. Stillinger and T.A. Weber, *Computer simulation of local order in condensed phase of silicon*, Phys. Rev. B 31 (1985), pp. 5262–5271.
[26] M. Lundgren, N.L. Allan, and T. Cosgrove, *Wetting of water and water/ethanol droplets on a non-polar surface: A molecular dynamics study*, Langmuir 18 (2002), pp. 10462–10466.
[27] M. Barisik and A. Beskok, *Equilibrium molecular dynamics studies on nanoscale-confined fluids*, Microfluid. Nanofluid. 11 (2011), pp. 269–282.
[28] J.H. Park and N.R. Aluru, *Temperature-dependent wettability on a titanium dioxide surface*, Mol. Simul. 35 (2009), pp. 31–37.
[29] J.Y. Wang, S. Betelu, and B.M. Law, *Line tension approaching a first-order wetting transition: Experimental results from contact angle measurements*, Phys. Rev. E 63 (2001), p. 031601.
[30] M. Brinkmann, J. Kierfeld, and R. Lipowsky, *A general stability criterion for droplets on structured substrates*, J. Phys. A: Math. General 37 (2004), p. 11547.
[31] T. Pompe and S. Herminghaus, *Three-phase contact line energetics from nanoscale liquid surface topographies*, Phys. Rev. Lett. 85 (2000), pp. 1930–1933.